OMAE2023-101218

PITCH MOTION CONTROL OF SPAR-TYPE FLOATING WIND TURBINES

Shuang-Rui Yu
Department of Naval Architecture, Ocean and Marine Engineering, University of Strathclyde
Glasgow, UK

Ming Zhang
Department of Naval Architecture, Ocean and Marine Engineering, University of Strathclyde
Glasgow, UK

Ming-Lu Chen
School of Naval Architecture and Ocean Engineering, Jiangsu University of Science and Technology
Zhenjiang, China

Zhi-Ming Yuan
Department of Naval Architecture, Ocean and Marine Engineering, University of Strathclyde
Glasgow, UK

ABSTRACT

Wave-induced pitch motion has adverse effects on the power generation of Floating Wind Turbines (FWTs). The traditional blade-pitch system, which is commonly used for regulating wind energy capture and power generation, can also be utilized to reduce the platform pitch motion. However, frequent active blade pitching can harm the wind turbine's blade-pitch bearing and gear system, leading to inevitable deficiencies in controlling such wave-induced pitch motion. Many structural control methods have been proposed to mitigate the motion of floating substructures. The present study proposes an active structural control method utilizing a plate hinged at the bottom of a spar-type floating substructure as an external control device. The damping force provided by the hydraulic Power Take Off (PTO) system between the spar and the plate serves as the control force during optimization. The controller is developed under an optimal declutching control framework, in which the damping coefficient of the PTO system is set as a binary function. It is found that current optimal declutching control strategy can effectively minimize the pitch motion of the spar-type substructure and maximize the PTO's power simultaneously. This indicates that more mechanical energy of the spar has been converted into electric energy. The proposed controller is able to reduce the wave-induced pitch motion by more than 21% and increase the PTO power capture by more than 370% at the platform's natural frequency than without control.

Keywords: floating wind turbine, wave-induced motion, declutching control, hydraulic power take off, optimal control theory

1. INTRODUCTION

The size of floating wind turbines is growing larger and larger. To capture more wind energy, the locations of FWTs are moving to deeper seas, where the average wind speed is higher, making wind power generation more economically feasible. In deep seas, the FWTs will suffer large and high-frequency wave force, and the large wave-induced motions could lead to severe consequences. The wave-induced motions will cause the reduction of blade swept area, and therefore the reduction of power output of wind turbines. For the spar-type FWT shown in Fig. 1, the platform motion in pitch direction is the main motion. Pitch motion may cause a large bending moment of the tower, and a potential oil leak.

FIGURE 1: THE HYWIND CONCEPT FLOATING WIND TURBINE [1].

Traditional blade pitch controller or generator torque controller of FWTs is mainly used to maximize the extraction of wind energy and reduce the fluctuation of power output. They have deficiencies when applied to mitigate wave-induced motion [1–3]. Wave frequency is much higher than the frequency that wind speed or wind direction changes. The period of sea waves can be in the order of seconds. Frequent blade pitching or

changes in generator torque can be harmful to the blade root's gear and bearing system, the main shaft, and the gearbox.

An alternative way is to use active structural control methods. Learning from the experience in civil engineering to avoid vibration, Tuned Mass Damper (TMD) [4,5] or Tuned Liquid Column Damper (TLCD) [6] were applied to the control methods. The dampers are placed in the nacelle with an active control device to provide a periodic force to reduce the pitch motion of substructures. There was an attempt of adding active mooring line force by the Sewing-thread Artificial Muscle (STAM) to control the motion, which can be only applied on the FWTs with a Tension Leg Platform (TLP) [7]. In this paper, we propose a hinged plate as the new type of active external control actuator to mitigate the motion of substructures.

In order to reduce the motion and extract more energy with this system, declutching control is introduced to tune the phase between the spar-type floating substructure and the plate. The concept of declutching control was first introduced by Salter in 2002 [8] as a complement to latching control. In 2009, Babarit [9] applied it to Wave Energy Converter (WEC) and compared its performance with that of pseudo-continuous control. The declutching control system provides discrete damping force by switching on and off alternatively the bypass valve in the circuit of the hydraulic cylinder. When the control command is 0, the by-pass valve is closed, and the damping force remains constant; when the control command is 1, the by-pass valve is open, and the damping force is reduced to 0. In the research on a hemispherical WEC [10], the amplification ratio of absorbed power by declutching control is less than 1.1. Li *et al.* implemented a real-time declutching control to a bi-oscillator WEC to enhance power capture [11]. Their research focuses on the implementation of the developed wave force prediction algorithm based on artificial neural networks and power extraction. The power absorption is significantly enhanced, but the motion of the outer oscillator is not well analysed. From these studies, it can be inferred that declutching control is particularly applicable to multiple bodies under certain conditions.

The present study proposes a novel concept of a hinged spar-plate system. With the hinged plate, the declutching control algorithm can extract mechanical energy from the floating substructures. The wave-induced motion is reduced accordingly, and the mechanical energy is transferred into electric energy. The effect of optimal declutching control on this hinged spar-plate system is studied. Two performance indicators, the average pitch speed of the spar-type floating substructure and the average power absorption of the PTO system, are investigated to evaluate the control effect.

2. MODELING OF HINGED SPAR-PLATE SYSTEM

2.1 Hinged spar-plate model

The computational model includes two rigid bodies: a spar-type floating substructure and a rectangular plate with a notch. The plate is hinged at the bottom of the spar. Since the main objective is to reduce the wave-induced pitch motion, and the frequency of wind speed fluctuation is much lower, the wind

turbine mounted on the floating substructure is neglected. The front view, side view, and dimensions of the hinged system model are illustrated in Fig. 2. The parameters of the spar-type floating substructure and the plate are listed in Table 1. A PTO device is installed at the hinge point to absorb energy from the relative pitch motion between the floating substructure and the plate.
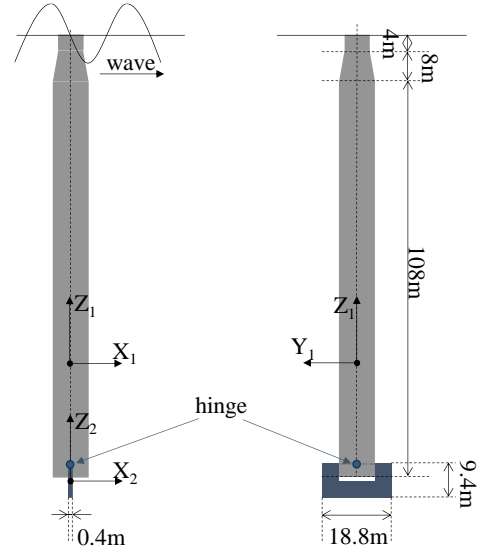
FIGURE 2: FRONT VIEW (LEFT) AND SIDE VIEW (RIGHT) OF THE HINGED SPAR-PLATE SYSTEM.

TABLE 1: DIMENSIONS OF THE SPAR-TYPE FLOATING SUBSTRUCTURE AND THE PLATE [12].

| Parameters	Dimensions
Depth to the Substructure Base Below SWL (Total Draft)	120 m
Depth to the Top of Taper Below SWL	4 m
Depth to the Bottom of Taper Below SWL	12 m
Substructure Diameter Above the Taper	6.5 m
Substructure Diameter Below the Taper	9.4 m
Substructure Mass, Including Ballast	8,029,202 kg
CM Location Below SWL Along Substructure Centreline	89.9155 m
Substructure Pitch Inertia about CM	4,229,230,000 kg·m^2
Substructure Pitch Nature frequency	0.36 rad/s
Plate Length	9.4 m
Plate Width	18.8 m

A full-scale multibody model including the spar-type floating substructure and the plate, but without the hinge, is established in WADAM [13] to obtain their hydrodynamic parameters. The body-fixed coordinate origins are located at the centre of gravity (CoG) of each body respectively. The wave propagates along the positive *X* axis.

Copyright © 2023 by ASME

2.2 Motion equation

The linear motion equation of the spar-plate system in the time domain is shown as follows:

$$\begin{bmatrix} M^a + m^a & m^{ab} \\ m^{ba} & M^b + m^b \end{bmatrix} \cdot \begin{bmatrix} \ddot{x}^a \\ \ddot{x}^b \end{bmatrix} + \begin{bmatrix} B^a & B^{ab} \\ B^{ba} & B^b \end{bmatrix} \cdot \begin{bmatrix} \dot{x}^a \\ \dot{x}^b \end{bmatrix}$$
$$+ \begin{bmatrix} K^a & 0 \\ 0 & K^b \end{bmatrix} \cdot \begin{bmatrix} x^a \\ x^b \end{bmatrix} = \begin{bmatrix} F^a + f_h^a \\ F^b + f_h^b \end{bmatrix} \tag{1}$$

where $x^a = [x_1^a \ \ x_2^a \ \ x_3^a \ \ x_4^a \ \ x_5^a \ \ x_6^a]^T$ are the 6-DoF motions of the spar-type floating substructure: surge, sway, heave, roll, and yaw; x^b are the 6-DoF motions of the plate; $\dot{x}^a$ are the 6-DoF velocities of the spar-type floating substructure: u, v, w, p, q, and r; $\ddot{x}^a$ are the 6-DoF accelerations of the spar-type floating substructure: $\dot{u}$, $\dot{v}$, $\dot{w}$, $\dot{p}$, $\dot{q}$, and $\dot{r}$. M^a, m^a, B^a, K^a, F^a, f_h^a are respectively the body mass, added mass, potential damping, restoring matrix, excitation force and hinge force of the spar-type floating substructure; M^b, m^b, B^b, K^b, F^b, f_h^b represent the parameters of the plate. This equation does not include the radiation force, which is the non-linear component.
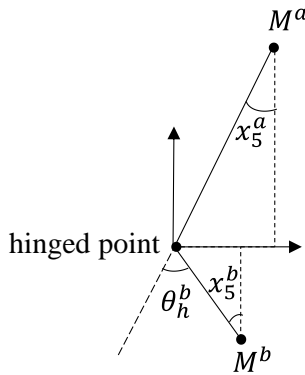
FIGURE 3: RELATIONSHIP OF PITCH MOTION AT THE HINGE POINT.

Because of the constraints at the hinge point, there are no relative motions in the surge, sway, heave, roll, and yaw directions at the hinge point. The hinge constrains the motions at the hinge point of the two bodies to be the same, except for the pitch direction. As illustrated in Fig. 3, the relative rotational angle at the hinge point of the two hinged bodies can be calculated from the difference between their respective pitch angles in the body-fixed coordinate, therefore, the constraint equations are shown as follows:

$$\begin{bmatrix} x_1^b \\ x_2^b \\ x_3^b \\ x_4^b \\ x_5^b \\ x_6^b \end{bmatrix} = \begin{bmatrix} 1 & 0 & 0 & 0 & R+r & 0 \\ 0 & 1 & 0 & R+r & 0 & 0 \\ 0 & 0 & 1 & 0 & 0 & 0 \\ 0 & 0 & 0 & 1 & 0 & 0 \\ 0 & 0 & 0 & 0 & 1 & 0 \\ 0 & 0 & 0 & 0 & 0 & 1 \end{bmatrix} \cdot \begin{bmatrix} x_1^a \\ x_2^a \\ x_3^a \\ x_4^a \\ x_5^a \\ x_6^a \end{bmatrix}$$
$$+ \begin{bmatrix} -r \\ 0 \\ 0 \\ 0 \\ 1 \\ 0 \end{bmatrix} \theta_h^b = S_{21} x^a + S_{22} \theta_h^b \tag{2}$$

where the motions of plate x^b can be represented by the motions of spar-type floating substructure x^a and the relative pitch angle θ_h^b. The matrix form can be rewritten as:

$$\begin{bmatrix} x^a \\ x^b \end{bmatrix} = \begin{bmatrix} I & 0 \\ S_{21} & S_{22} \end{bmatrix} \cdot \begin{bmatrix} x^a \\ \theta_h^b \end{bmatrix} = S \cdot \begin{bmatrix} x^a \\ \theta_h^b \end{bmatrix} \tag{3}$$

where S is the coefficient matrix of hinge constraints. In the motion equation of the system, x^b, $\dot{x}^b$, $\ddot{x}^b$ can be replaced by x^a, $\dot{x}^a$, $\ddot{x}^a$ and θ_h^b, $\dot{\theta}_h^b$, $\ddot{\theta}_h^b$, so the original 12-DoF Equation set (1) can be transformed into a 7-DoF equation set:

$$S^T \begin{bmatrix} M^a + m^a & m^{ab} \\ m^{ba} & M^b + m^b \end{bmatrix} \cdot S \begin{bmatrix} \ddot{x}^a \\ \ddot{\theta}_h^b \end{bmatrix}$$
$$+ S^T \begin{bmatrix} B^a & B^{ab} \\ B^{ba} & B^b \end{bmatrix} \cdot S \begin{bmatrix} \dot{x}^a \\ \dot{\theta}_h^b \end{bmatrix} + S^T \begin{bmatrix} K^a & 0 \\ 0 & K^b \end{bmatrix} \cdot S \begin{bmatrix} x^a \\ \theta_h^b \end{bmatrix}$$
$$= S^T \begin{bmatrix} F^a \\ F^b \end{bmatrix} \tag{4}$$

where f_h^a and f_h^b have been eliminated due to Newton's third law.

2.3 State-space representation

In the time domain, the non-linear radiation term in the motion equation can be derived from Cummins' impulse theory [14]. According to Cummins' equation, the radiation force is:

$$f^R(t) = \int_0^t h(t-\tau)\dot{x}(\tau)d\tau \tag{5}$$

$h(t)$ is the retardation kernel function, representing the wave memory effect. $h(t)$ can be obtained from the added mass or potential damping in the frequency domain:

$$h(t) = \frac{2}{\pi} \int_0^\infty \omega\big(m - \mu(\omega)\big) \sin(\omega t)\, d\omega =$$
$$\frac{2}{\pi} \int_0^\infty \lambda(\omega) \cos(\omega t)\, d\omega \tag{6}$$

$h(s)$, the Laplace transform of $h(t)$, can be regarded as the transfer function from the velocity $\dot{x}(s)$ to the radiation force $f^R(s)$. It can also be approximated with polynomial equations, and represented in the state-space form:

$$f^R(t) = \boldsymbol{C_r} \cdot \boldsymbol{u}(t)$$
$$\dot{\boldsymbol{u}}(t) = \boldsymbol{A_r} \cdot \boldsymbol{u}(t) + \boldsymbol{B_r} \dot{x}(t) \tag{7}$$

The system matrices $\boldsymbol{A_r}$, $\boldsymbol{B_r}$ and $\boldsymbol{C_r}$ are derived by frequency-domain identification (FDI) using the MSS FDI toolbox [15]. Hence, when considering the wave surface memory effect, Equation (4) can be written as:

$$S^T \begin{bmatrix} M^a + m^a & m^{ab} \\ m^{ba} & M^b + m^b \end{bmatrix} \cdot S \begin{bmatrix} \ddot{x}^a \\ \ddot{\theta}_h^b \end{bmatrix} +$$
$$S^T \begin{bmatrix} B^a & B^{ab} \\ B^{ba} & B^b \end{bmatrix} \cdot S \begin{bmatrix} \dot{x}^a \\ \dot{\theta}_h^b \end{bmatrix} +$$
$$S^T \begin{bmatrix} C_r^{aa} & C_r^{ab} & 0 & 0 \\ 0 & 0 & C_r^{bb} & C_r^{ba} \end{bmatrix} \cdot \begin{bmatrix} u^{aa} \\ u^{ab} \\ u^{bb} \\ u^{ba} \end{bmatrix} +$$
$$S^T \begin{bmatrix} K^a & 0 \\ 0 & K^b \end{bmatrix} \cdot S \begin{bmatrix} x^a \\ \theta_h^b \end{bmatrix} = S^T \begin{bmatrix} F^a \\ F^b \end{bmatrix},$$
$$\begin{bmatrix} \dot{u}^{aa} \\ \dot{u}^{ab} \\ \dot{u}^{bb} \\ \dot{u}^{ba} \end{bmatrix} = \begin{bmatrix} A_r^{aa} & 0 & 0 & 0 \\ 0 & A_r^{ab} & 0 & 0 \\ 0 & 0 & A_r^{bb} & 0 \\ 0 & 0 & 0 & A_r^{ba} \end{bmatrix} \cdot \begin{bmatrix} u^{aa} \\ u^{ab} \\ u^{bb} \\ u^{ba} \end{bmatrix} +$$
$$\begin{bmatrix} B_r^{aa} & 0 \\ 0 & B_r^{ab} \\ 0 & B_r^{bb} \\ B_r^{ba} & 0 \end{bmatrix} S \begin{bmatrix} \dot{x}^a \\ \dot{\theta}_h^b \end{bmatrix} \tag{8}$$

The comparison of radiation forces of the spar-type floating substructure and the plate is shown in Fig. 4. The radiation ratio is the ratio of radiation force and wave excitation force. Since the waterplane area of the model is relatively small in engineering applications, the radiation ratio is small in most wave frequencies. The radiation ratio becomes large only when the wave frequency is near the natural frequency, 0.36 rad/s.

Define $\boldsymbol{y} = \left[x^a, \theta_h^b, \dot{x}^a, \dot{\theta}_h^b, u^{aa}, u^{ab}, u^{bb}, u^{ba}\right]^T$ as the state vector in the state space. The state-space representation of Equation (8) can be re-expressed as:

$$\dot{\boldsymbol{y}} = \gamma \cdot \boldsymbol{y} + \eta$$

$$\gamma = \begin{bmatrix} 0 & \Lambda & 0 \\ -\dfrac{S^T K S}{S^T M S} & -\dfrac{S^T B S}{S^T M S} & -\dfrac{S^T C_r}{S^T M S} \\ 0 & B_r S & A_r \end{bmatrix},$$
$$\eta = \begin{bmatrix} 0 \\ -\dfrac{F}{S^T M S} \\ 0 \end{bmatrix} \tag{9}$$

This linearized representation of motion equation can be solved with the 4th-order Runge Kutta method in MATLAB.
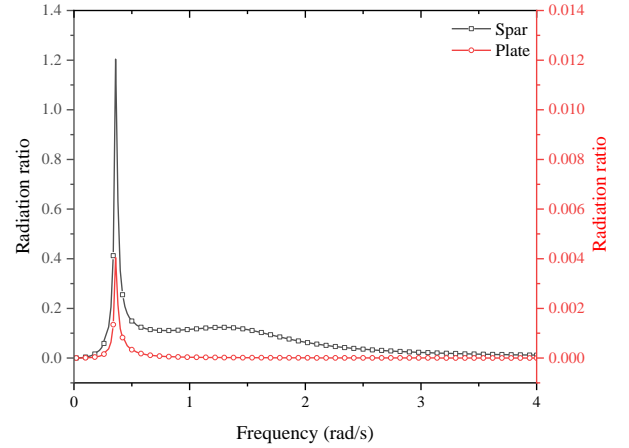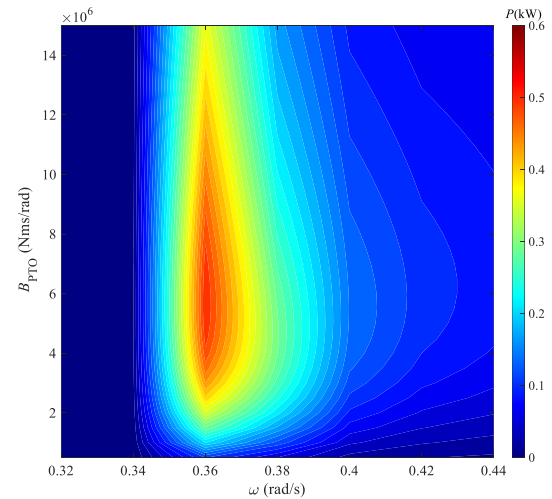

FIGURE 4: RADIATION RATIO OF THE SPAR AND THE PLATE UNDER DIFFERENT FREQUENCIES.

2.4 PTO System
The damping of the PTO device only exists in the pitch direction. The hydraulic PTO force is approximate to friction (Coulomb) damping form, which is shown as follows:

$$P = B_{\text{PTO}} \dot{\theta}_h^{b\,2} \tag{10}$$

FIGURE 5: POWER ABSORPTION UNDER DIFFERENT PTO DAMPING COEFFICIENTS AND WAVE FREQUENCIES.

Copyright © 2023 by ASME

The average power absorption of the PTO system is determined by two factors: the damping coefficient, B_{PTO}, and the relative angular velocity at the hinge point, $\dot{\theta}_h^b$. However, these two factors also influence each other. The relative angular velocity can be reduced by increasing the damping coefficient of PTO. Figure 5 compares the power absorption under different damping coefficients and regular wave frequencies. As shown in this figure, the power is maximized when B_{PTO} is 5.5×10^6 N·m·s/rad. This value of the damping coefficient is considered the best PTO configuration of the hinged spar-plate system without control.

3. CONTROL METHODOLOGY

3.1 Declutching control

The declutching control system provides a discrete damping force of $B_{PTO}\dot{\theta}_h^b$ and 0 alternatively. Figure 6 shows an example of the time history of the PTO damping coefficient in declutching control.
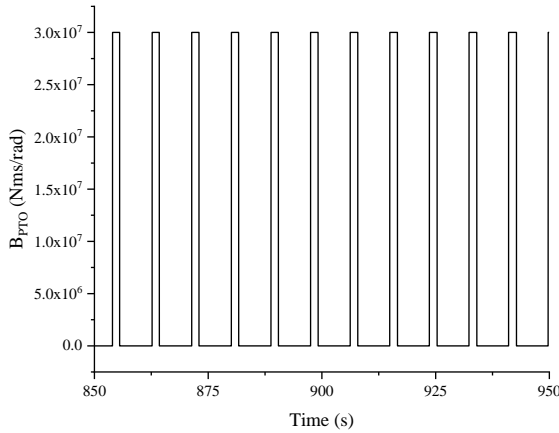
FIGURE 6: TIME HISTORY OF THE PTO DAMPING COEFFCIENT UNDER OPTIMAL DECLUCHING CONTROL.

By tuning the system's natural frequency to match the wave frequency and allowing the resonance to occur, declutching control can enhance the efficiency of power take-off system in certain wave frequencies. When declutching control is activated, the PTO is switched off and the structures are allowed to accelerate freely. It can reduce the average damping of the system and increase its natural frequency. Declutching control is applicable when the wave frequency is higher than the system's natural frequency.

3.2 Pontryagin's maximum principle

Pontryagin's maximum principle (PMP) is a widely used theory in optimal control. In this research, it is used to determine the minimum motion of floating bodies or the maximum power absorption of PTO devices within a limited time period using the proposed control.

When the binary control command, β, is introduced to Equation (9), the γ in the motion equation with control can be derived as follows:

$$\gamma = \begin{bmatrix} \mathbf{0} & \mathbf{\Lambda} & \mathbf{0} \\ -\dfrac{S^T K S}{S^T M S} & -\dfrac{S^T(BS+B_{PTO}+\beta B_c)}{S^T M S} & -\dfrac{S^T C_r}{S^T M S} \\ \mathbf{0} & \mathbf{B_r}S & \mathbf{A_r} \end{bmatrix} \quad (11)$$

where B_c is equal to $-B_{PTO}$, so when β is 0, PTO works normally; when β is 1, the damping of PTO will be offloaded.

In order to minimize or maximize the target cost function, we need to minimize or maximize the Hamiltonian, H, calculated by the state of the system:

$$H = L + \lambda(\gamma \cdot \mathbf{y} + \eta)$$
$$\dot{\lambda} = -\frac{\partial H}{\partial \mathbf{y}} = -\frac{\partial L}{\partial \mathbf{y}} - \lambda\gamma \quad (12)$$

where λ is the Lagrange multiplier and L is the performance index. We define L as $|q^a|$, which represents the pitch speed of the spar-type floating substructure in this paper. By solving the value of λ, the Hamiltonian H containing β can be derived. In discrete control, the control command β is binary, which means the command can be either 0 or 1. When the sign of the coefficient before β is negative, β is set to be 0; when the sign is positive, β is 1. Hence, H can be maximized.

4. RESULTS AND DISCUSSION

The characteristics of the motion amplitude and power absorption of the multibody system are investigated under regular waves. The wave excitation forces are assumed to be sinusoidal, which are defined as:

$$F_{w,i} = A f_i^\alpha \cos\left(\omega_w t + \phi_i^p\right), i = 1,2,\dots,6 \quad (13)$$

where A is the incident wave amplitude; f_i^α is the wave force transfer function of harmonic waves; ω_w is the circular wave frequency; ϕ_i^p is the phase angle of harmonic waves.

The simulation of the optimal control is conducted in MATLAB, and several performance indicators are monitored. The cost function q_{avg}^a is the average pitch speed of the spar-type floating substructure, which is defined as follows:

$$q_{avg}^a = \frac{1}{T}\int_0^T |q^a| dt \quad (14)$$

P_{avg} is the average power absorption of PTO, which is defined as follows:

$$P_{avg} = \frac{1}{T}\int_0^T B_{PTO}\dot{\theta}_h^{b^2} dt \quad (15)$$

The standard deviation of q^a, which represents the platform pitch velocity, is defined as follows:

$$S^a = \sqrt{\frac{\sum_{i=1}^{N}(q_i^a - q_{avg}^a)^2}{N-1}} \qquad (16)$$

where N is the number of the data points; q_i^a is each of the values of the platform pitch velocity. Besides, P_{avg} can be non-dimensionalised to the capture width ratio (CWR), which is defined as follows:

$$CWR[\%] = \frac{P_{avg}}{JB} \times 100 \qquad (17)$$

where $J = \frac{1}{2}\rho g A^2 \left(\frac{1}{2}\frac{g}{\omega}\right)$ is the mean wave energy flux given power per wavefront in deep water (W/m), and the wave amplitude A is set as 0.1m; B is the characteristic length of the spar-type floating substructure and set as 6.5m.

### 4.1 Control effect in regular waves

The power absorption of PTO is compared under different wave frequencies and damping coefficients in Fig.7. The peak of power absorption in this figure gives a guide for selecting the best initial configuration in this section. The results of optimal declutching control when B_{PTO} is 3×10^7 N·m·s/rad and ω is 0.36 rad/s are shown in Fig. 9-11.
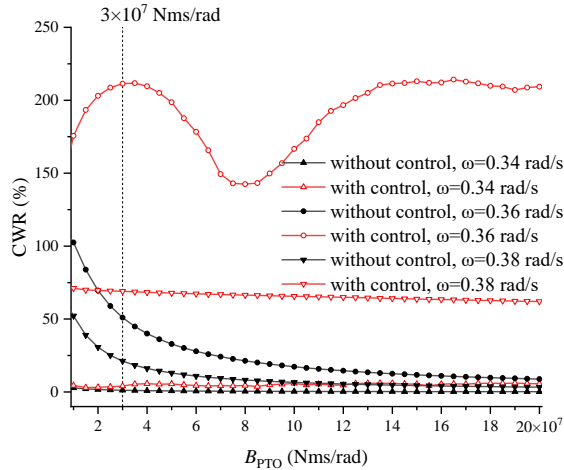

FIGURE 7: RELATIONSHIP OF THE AVERAGE PTO POWER ABSORPTION AND THE DAMPING COEFFICIENTS IN DIFFERENT WAVE FREQUENCIES.

It could be found in Fig. 8 that the performance index S^a is well optimized under current optimal declutching control method. S^a reduces by 21.34% with control. Besides, another performance index investigated herein, P_{avg}, is also enhanced as a "by-product". J is 68.03W/m in current configuration, so $CWR = P_{avg}/442.18 \times 100$. Current control method can enhance CWR by 371.79%. CWR is possible to be larger than

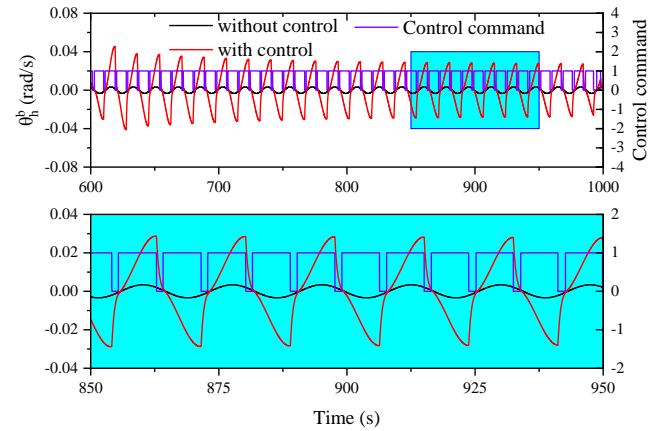100% because the wave energy can come from beyond the body width.
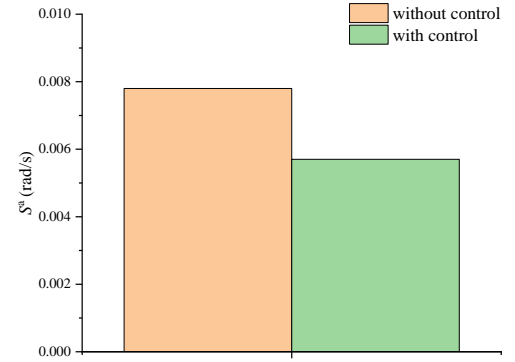
(a) STANDARD DEVIATION OF THE PITCH SPEED OF THE SPAR-TYPE FLOATING SUBSTRUCTURE.
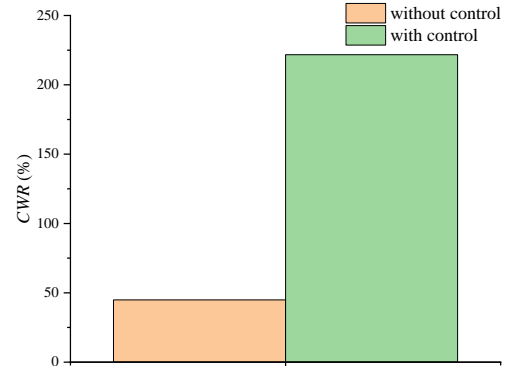
(b) CAPTURE WIDTH RATIO OF THE PTO.

FIGURE 8: PERFORMANCE INDICES WHEN DECLUTCHING CONTROL IS APPLIED TO THE SPAR-PLATE SYSTEM.


FIGURE 9: TIME HISTORY OF THE RELATIVE ANGULAR VELOCITY WITHOUT AND WITH THE DECLUTCHING CONTROL.

The time history result of the declutching control is shown in Fig. 9. The response under the optimal declutching control is also periodic after convergence. Since the average damping of declutching control is relatively lower, the system's motion

6

response needs a longer time to converge, so we select 600-1000 seconds in the whole simulation time.

In Fig. 9, when the command control is 1 (activated), the PTO is switched off and the damping force is 0 constantly. The relative angular velocity surges in a short time without the constraint of damping. The mechanical energy of the plate accumulates until its velocity is large enough. Then the PTO is switched on again when the command control returns to 0 (unactivated). The damping force is reloaded, and the PTO begins to extract mechanical energy again.
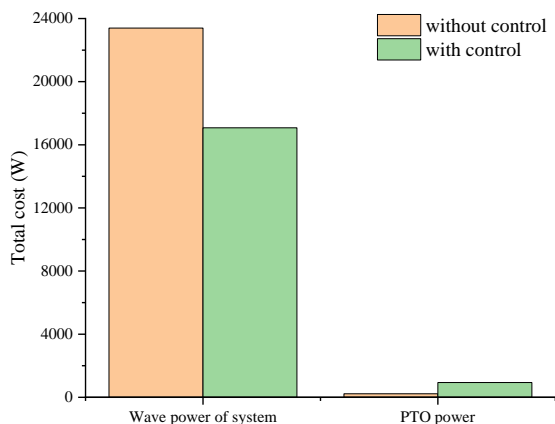
FIGURE 10: THE VARIATION OF WAVE POWER (LEFT) AND PTO POWER (RIGHT) UNDER CONTROL.
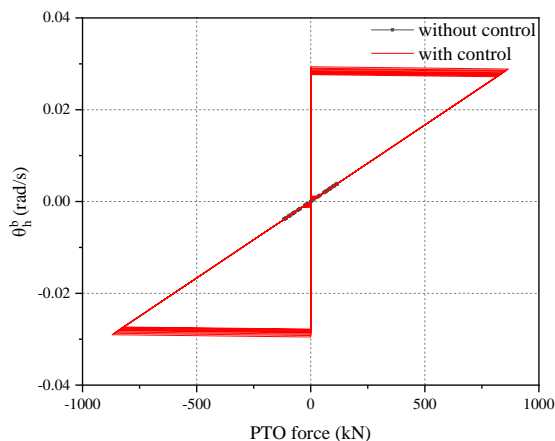
FIGURE 11: PHASE PLOT OF RELATIVE ANGULAR PITCH VELOCITIES AND DAMPING FORCE OF PTO.

The mechanical energy of the spar-type substructure comes from wave energy. The total wave power is calculated as the average value of the product of the excitation wave forces F_w and the body velocity $\dot{x}$ over a computational period. We can find in Fig. 10 that 5.47% of the wave energy is converted into electric energy under optimal declutching control, which is 4.51% higher than results without control. The hinged spar-plate system can effectively absorb wave energy under the current control method. The total power absorbed from wave energy is reduced with optimal declutching control. However, the power absorption of the PTO system has been increased. This indicates

that the percentage of energy converted to electric energy is enhanced with this control method.

Figure 11 shows the relationship of phases between the PTO damping force and the relative angular velocity. The area under the curves, which represents the power of PTO force, has significantly increased.

4.2 Control effect under different frequencies

The natural frequency of the spar can hardly be influenced by the hinged plate or B_{PTO} when the plate is very small. In Fig. 12(a), the motion amplitude of the spar peaks when the wave frequency reaches its natural frequency, which is the resonance frequency. When resonance happens, the maximum percentage of wave energy is absorbed and converted into mechanical energy.
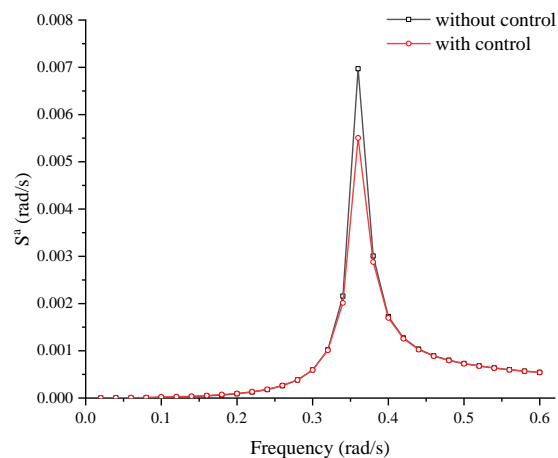
(a) STANDARD DEVIATION OF THE PITCH SPEED OF THE SPAR-TYPE FLOATING SUBSTRUCTURE.
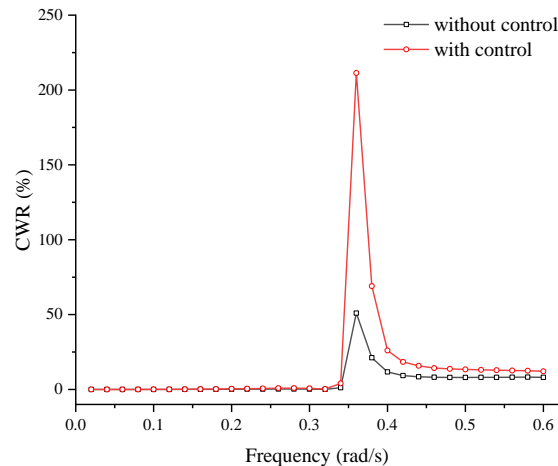
(b) CAPTURE WIDTH RATIO OF THE PTO.

FIGURE 12: PERFORMANCE INDICES UNDER DIFFERENT WAVE FREQUENCIES.

As shown in Fig.12(b), the declutching control has a greater influence in enhancing power absorption when wave frequency is close to or above the resonance frequency, while there is no significant improvement at low frequencies. This is because the

undamped PTO enables the plate to accelerate immediately to "catch up" the phase of wave force, making the method more effective in high-frequency waves. During declutching control, the PTO system is undamped occasionally, so the average PTO damping decreases. When the damping ratio of a system is reduced, its resonance frequency will increase and match the wave frequency.

The results in different wave frequencies indicate that the maximum platform pitch motion near the natural frequency can be effectively reduced, while the motion in other frequencies stays small. The reduced kinetic energy is converted to electric power, which can be observed from the enhancement of PTO power absorption. If a wind turbine is mounted on the spar-type floating substructure, there will be additional fluctuating thrust force acting on the substructure and coupling between aerodynamic and hydrodynamic forces, which will not be discussed in this paper due to their complexity.

5. CONCLUSION

The current study applies an optimal declutching control method to a novel hinged spar-plate system, in which the plate is hinged at the bottom of the spar-type substructure to reduce its pitch motion. Hydrodynamic responses and power absorption of the hinged spar-plate system have been analysed. The declutching control allows the hinged plate to gain larger acceleration, therefore, the PTO system can convert more mechanical energy to electrical energy compared to the system without control.

The declutching control is applicable to multiple bodies when the wave frequency is higher. With the configuration of PTO damping coefficient B_{PTO} and the wave frequency ω in this paper, the application of optimal declutching control has resulted in a reduction of more than 21% in the standard deviation of the average pitch speed of spar-type floating substructure S^a, and an increase of more than 370% in the capture width ratio of PTO CWR. The plate can "catch up" the wave when declutching control is activated and the PTO damping is offloaded. The reduced motion of the spar-type substructure will benefit the power output of the mounted wind turbine. Using a small plate as an external control device can be a practical and cost-effective solution for stabilising large FWTs in the future.

ACKNOWLEDGEMENTS

REFERENCES

[1] Skaare, B., Nielsen, F. G., Hanson, T. D., Yttervik, R., Havmøller, O., and Rekdal, A., 2015, "Analysis of Measurements and Simulations from the Hywind Demo Floating Wind Turbine," Wind Energy, **18**(6), pp. 1105–1122.

[2] Larsen, T. J., and Hanson, T. D., 2007, "A Method to Avoid Negative Damped Low Frequent Tower Vibrations for a Floating, Pitch Controlled Wind Turbine," *Journal of Physics: Conference Series*, Institute of Physics Publishing.

[3] Skaare, B., David Hanson, T., Gunnar Nielsen, F., Yttervik, R., Melchior Hansen, A., Thomsen, K., and Juul Larsen, T., 2007, "Integrated Dynamic Analysis of Floating Offshore Wind Turbines," *European Wind Energy Conference and Exhibition*, pp. 1929–1939.

[4] Namik, H., Rotea, M., and Lackner, M., 2013, "Active Structural Control with Actuator Dynamics on a Floating Wind Turbine," *51st AIAA Aerospace Sciences Meeting Including the New Horizons Forum and Aerospace Exposition*, American Institute of Aeronautics and Astronautics, Reston, Virigina, p. 455.

[5] Mu, A., Huang, Z., Liu, A., Wang, J., Yang, B., and Qian, Y., 2022, "Optimal Model Reference Adaptive Control of Spar-Type Floating Wind Turbine Based on Simulated Annealing Algorithm," Ocean Engineering, **255**.

[6] Coudurier, C., Lepreux, O., and Petit, N., 2015, "Passive and Semi-Active Control of an Offshore Floating Wind Turbine Using a Tuned Liquid Column Damper," *IFAC-PapersOnLine*, pp. 241–247.

[7] Li, Y., and Wu, Z., 2016, "Stabilization of Floating Offshore Wind Turbines by Artificial Muscle Based Active Mooring Line Force Control," *Proceedings of the American Control Conference*, Institute of Electrical and Electronics Engineers Inc., pp. 2277–2282.

[8] Salter, S. H., Taylor, J. R. M., and Caldwell, N. J., 2002, "Power Conversion Mechanisms for Wave Energy," Proceedings of the Institution of Mechanical Engineers, Part M: Journal of Engineering for the Maritime Environment, **216**(1), pp. 1–27.

[9] Babarit, A., Guglielmi, M., and Clement, A. H., 2009, "Declutching Control of a Wave Energy Converter," Ocean Engineering, **36**, pp. 12–13.

[10] Zhang, X.-T., Yang, J.-M., and Xiao, L.-F., 2014, "Declutching Control of a Point Absorber with Direct Linear Electric PTO Systems," Ocean Systems Engineering, **4**(1), pp. 63–82.

[11] Li, L., Gao, Y., Ning, D. Z., and Yuan, Z. M., 2021, "Development of a Constraint Non-Causal Wave Energy Control Algorithm Based on Artificial Intelligence," Renewable and Sustainable Energy Reviews, **138**.

[12] Jonkman, J., 2010, *Definition of the Floating System for Phase IV of OC3*.

[13] DNV GL, 2019, "WADAM-Wave Analysis by Diffraction and Morison Theory."

[14] Cummins, W. E., 1962, *The Impulse Response Function and Ship Motions*, WASHINGTON D C.

[15] Fossen, T. I., 2011, *Handbook of Marine Craft Hydrodynamics and Motion Control*, Wiley.